

Discovery of the First Selective Nanomolar Inhibitors of ERAP2 by Kinetic Target-Guided Synthesis

Virgyl Camberlein⁺, Charlotte Fléau⁺, Pierre Sierocki⁺, Lenong Li⁺, Ronan Gealageas, Damien Bosc, Valentin Guillaume, Sandrine Warengem, Florence Leroux, Melissa Rosell, Keguang Cheng, Laura Medve, Mathilde Prigent, Myriam Decanter, Catherine Piveteau, Alexandre Biela, Maxime Eveque, Julie Dumont, Anastasia Mpakali, Petros Giastas, Adrien Herledan, Cyril Couturier, Jörg Haupenthal, Laetitia Lesire, Anna K. H. Hirsch, Benoit Deprez, Efstratios Stratikos, Marlene Bouvier,* and Rebecca Deprez-Poulain*

Abstract: Endoplasmic reticulum aminopeptidase 2 (ERAP2) is a key enzyme involved in the trimming of antigenic peptides presented by Major Histocompatibility Complex class I. It is a target of growing interest for the treatment of autoimmune diseases and in cancer immunotherapy. However, the discovery of potent and selective ERAP2 inhibitors is highly challenging. Herein, we have used kinetic target-guided synthesis (KTGS) to identify such inhibitors. Co-crystallization experiments revealed the binding mode of three different inhibitors with increasing potency and selectivity over related enzymes. Selected analogues engage ERAP2 in cells and inhibit antigen presentation in a cellular context. **4d (BDM88951)** displays favorable in vitro ADME properties and in vivo exposure. In summary, KTGS allowed the discovery of the first nanomolar and selective highly promising ERAP2 inhibitors that pave the way of the exploration of the biological roles of this enzyme and provide lead compounds for drug discovery efforts.

Introduction

The endoplasmic reticulum aminopeptidases (ERAP1 and 2) are key enzymes in the generation of antigenic epitopes that bind the Major Histocompatibility Complex class I (MHC-I)^[1,2] (Figure 1). Therefore, they modulate the immunopeptidome presented at the cell surface that triggers the immune response via T- or NK-cells and thus appear as potential targets for autoimmune diseases, cancer immuno-

therapy or viral infections.^[3,4] ERAP1 is the most studied isoform but ERAP2 has recently aroused interest.^[5] ERAP2 is indeed a risk factor for three MHC-I associated diseases: ankylosing spondylitis,^[6] birdshot chorioretinopathy^[7] and psoriasis^[8] (Figure S1).

ERAP2 has also been shown to be implicated in viral infections and viral antigen presentation.^[9,10] Like ERAP1, ERAP2 expression in tumors can facilitate immune evasion and predicts the overall survival in cancer.^[11] Recent studies

[*] V. Camberlein,⁺ Dr. C. Fléau,⁺ Dr. P. Sierocki,⁺ Dr. R. Gealageas, Dr. D. Bosc, V. Guillaume, S. Warengem, Dr. F. Leroux, Dr. M. Rosell, Dr. K. Cheng, Dr. L. Medve, M. Prigent, M. Decanter, C. Piveteau, A. Biela, M. Eveque, J. Dumont, A. Herledan, Dr. C. Couturier, Dr. L. Lesire, Prof. B. Deprez, Prof. R. Deprez-Poulain
 Univ. Lille, Inserm, Institut Pasteur de Lille, U1177, Drugs and Molecules for Living Systems
 3 rue du Pr Laguesse, 59000 Lille (France)
 and
 European Genomic Institute for Diabetes, EGID, Pôle Recherche
 1 place de Verdun, 59045 Lille Cedex (France)
 E-mail: rebecca.deprez@univ-lille.fr

Dr. L. Li,⁺ Prof. M. Bouvier
 Department of Microbiology and Immunology,
 University of Illinois at Chicago
 909 S Wolcott Avenue, Chicago, IL 60612 (USA)
 E-mail: mbouvier@uic.edu

Dr. A. Mpakali, Dr. P. Giastas, Dr. E. Stratikos
 National Center for Scientific Research Demokritos
 Agia Paraskevi 15341 (Greece)

Dr. E. Stratikos
 Laboratory of Biochemistry, Department of Chemistry,
 National and Kapodistrian University of Athens
 Panepistimiopolis, Zographou 15784 (Greece)

Dr. J. Haupenthal, Prof. A. K. H. Hirsch
 Helmholtz Institute for Pharmaceutical Research Saarland (HIPS),
 Helmholtz Centre for Infection Research (HZI)
 Campus E8 1, 66123 Saarbrücken (Germany)

Prof. A. K. H. Hirsch
 Department for Pharmacy, Saarland University
 Campus E8 1, 66123 Saarbrücken (Germany)

[⁺] These authors contributed equally to this work.

© 2022 The Authors. Angewandte Chemie International Edition published by Wiley-VCH GmbH. This is an open access article under the terms of the Creative Commons Attribution Non-Commercial NoDerivs License, which permits use and distribution in any medium, provided the original work is properly cited, the use is non-commercial and no modifications or adaptations are made.

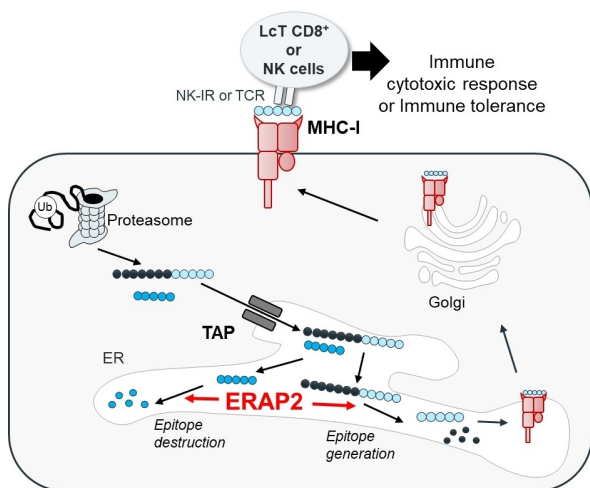


Figure 1. Function of ERAP2 in antigen trimming leading to either epitope destruction or generation.

have highlighted that low levels of ERAP2 can be associated with improved response to anti-PDL1 treated patients.^[12]

ERAP2 was initially discovered as an accessory protease to ERAP1^[13,14] with specific substrate preferences.^[15] Although several X-ray structures of ERAP2 have been determined^[16] and provided information useful for the rational design of inhibitors, so far, published ERAP2 inhibitors do not meet the requirements for a use as pharmacological probes or lead compounds for therapeutic intervention. They lack selectivity over ERAP1 or the related enzyme IRAP^[17] or display low potency^[18,19] (Figure S2). Indeed, most of ERAP2 inhibitors described derive of rationally designed phosphinic or aminobenzamide inhibitors of ERAP1 and/or IRAP. They also bear an amino group, mimicking the α -amino terminus of substrates of aminopeptidases. This amine engages in electrostatic interactions that displays low requirements for distance and orientation and as such is a rather promiscuous pharmacophore in the aminopeptidase family. For both of these reasons, the achievement of isoform selectivity is challenging

in these chemical series. There is thus a need for an alternative strategy to discover potent and selective ERAP2 inhibitors.

Kinetic target-guided synthesis (KTGS) uses the protein of interest as a template for the assembly of biocompatible reagents into its own ligands.^[21] Indeed, the protein synthesizes a “divalent” ligand by equilibrium-controlled selection of reagents with complementary reactive functions until an irreversible reaction links the pair of reagents that best fits the protein binding site in a reactive relative configuration. Having shown previously that KTGS can produce ligands which exploit protein flexibility and bind to previously unknown protein conformations through specific hydrogen bond and hydrophobic interactions,^[20] we hypothesized that we could identify specific ERAP2 ligands devoid of positive charge that harness subtle differences in conformation in the aminopeptidases family.

We describe hereafter the discovery of the first ligands by KTGS and the optimization leading to unprecedented nanomolar and selective ERAP2 inhibitors. Potency and selectivity data are rationalized using the X-ray structures of the enzyme-ligand complexes. Cellular activity and target engagement as well as pharmacokinetics qualify the best compounds from this series to address the roles of ERAP2 both in vitro and in vivo.

Results and Discussion

Discovery of ERAP2 Inhibitors by KTGS

We chose in situ click-chemistry, (Figure 2a) using biocompatible azides and alkynes, as the KTGS reaction. Six azides (**1a–1f**, Figure 2b), bearing a hydroxamic acid as zinc binding group (ZBG), and no amino group, were selected from an in house library and tested for their inhibition of ERAP2 (Figure S3). A large library of 175 alkynes, distributed in 18 clusters of 9 or 10 alkynes, was used to introduce diversity (Figure 2c). In total, 72 nine-to-one or ten-to-one mixtures of alkyne-azides were incubated with

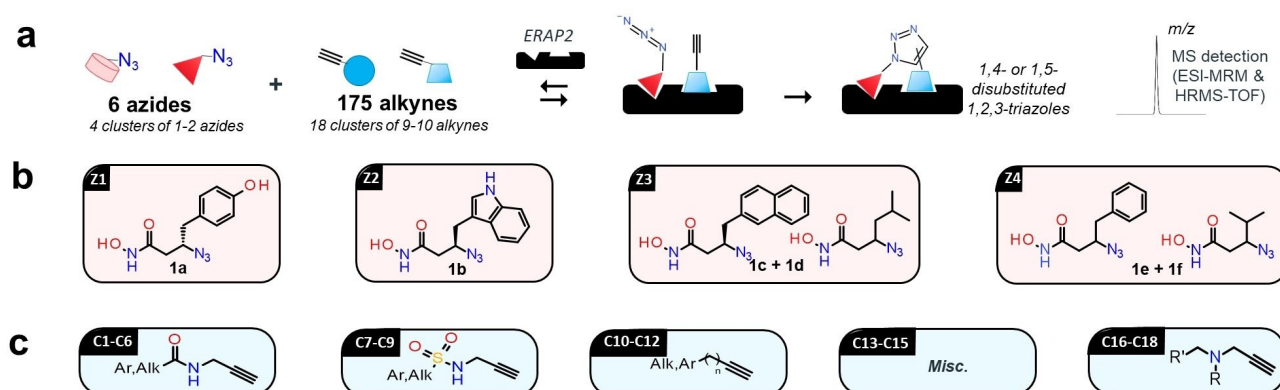


Figure 2. Design of the kinetic target-guided synthesis (KTGS) of ERAP2 ligands. a) function of ERAP2 in antigen trimming leading to either epitope destruction or generation; b) Principle of KTGS; c) Clusters of azides **1a–f** (**Z1–Z4**); d) Clusters of alkynes (**C1–C18**); *Misc.* miscellaneous

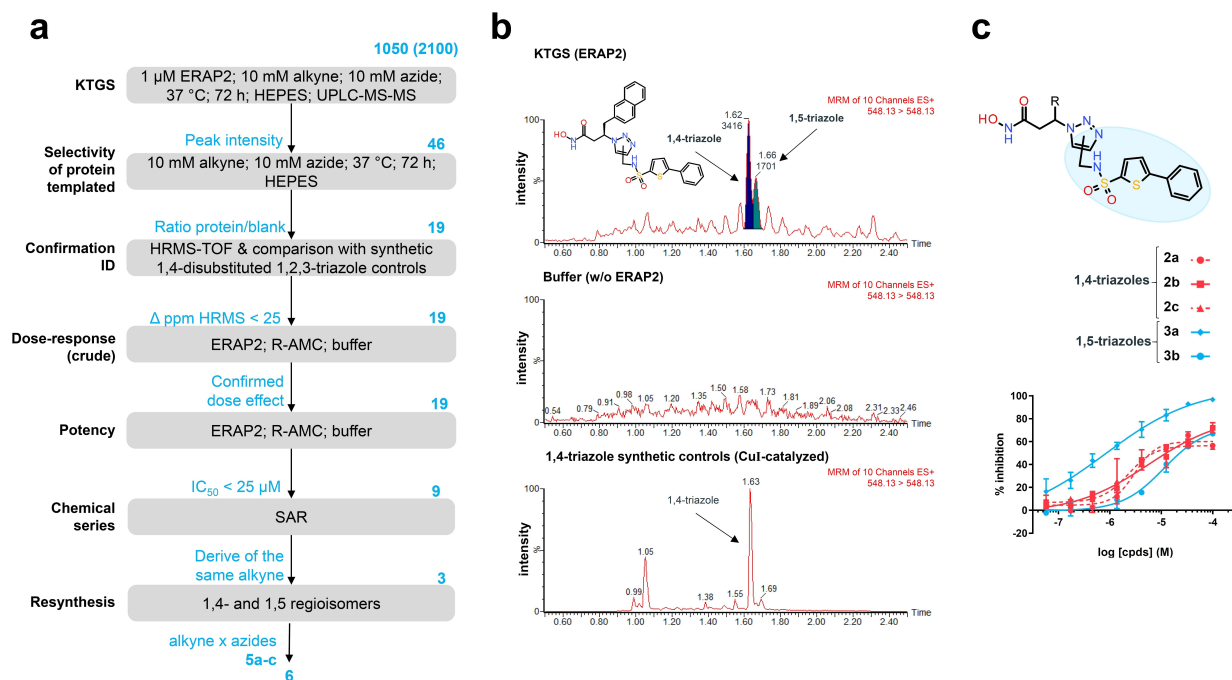


Figure 3. Discovery of ligands of ERAP2 by kinetic target-guided synthesis (KTGS). a) Flow chart for hit selection including KTGS, selectivity, confirmatory, dose-response assay and resynthesis. Selection criteria and number of compounds are given for each step. Overall 1050 combinations of azide-alkyne producing potentially 2100 triazoles including 1,4- and 1,5- regioisomers. b) Example of LCMS-MS chromatograms from KTGS (top); un-templated reaction mixture in buffer (middle); and 1,4-triazole synthetic control (bottom) c) Dose-response curves and structure for resynthesized hits **2a–c**; **3a–b**.

ERAP2 to give potentially 2100 products (1,4 and 1,5 disubstituted 1,2,3-triazoles (Figure 2a, S4).

We selected hits based on a seven-step selection flowchart (Figure 3a). KTGS mixtures were analyzed by mass spectrometry. The selectivity of the protein-templated formation of triazole was assessed by comparing KTGS samples with mixtures of azides and alkynes incubated in buffer in the absence of the protein. Identity of the triazoles was confirmed by comparison with synthetic 1,4-disubstituted triazoles controls and the chemical formula was checked by HRMS-TOF. 19 hits were identified, some of which being mixtures of both 1,5-triazole and 1,4 triazole regioisomers (Figure 3b). All hits displayed a dose-response effect and nine of them had an IC_{50} value below $25 \mu\text{M}$ (47 %, Figure S5a). Analysis of the clusters, revealed that almost one-third of the hits were derivatives of the precursor **1d** (Figure S5b) and alkynes bearing a sulfonamide moiety **C7–C9** (Figure S5c-d). In particular three hits originated from the same *N*-propargyl thiophene sulfonamide. We thus selected both 1,4- and 1,5-triazoles **2a–c** and **3a–c** in this series (Figure 3c, Table 1) for chemical synthesis. 1,5-triazoles **3a–c** were obtained using an intramolecular 1,3-dipolar cycloaddition (Supplementary methods). 1,4-triazoles **2a–c** were obtained by classical copper-catalyzed 1,3-dipolar cycloaddition (Supplementary methods).

The KTGS-hit 1,5-triazole **3a**, derived of phenol precursor **1a**, was the most potent hit with an IC_{50} value of $0.85 \mu\text{M}$, while its 1,4-triazole regioisomer **4a** displayed an IC_{50} value of $3.0 \mu\text{M}$ (Table 1).

Table 1: Inhibition of ERAP2 by KTGS hits **2a–c**, **3a–c**.^[a]

Cpd.	R1	IC_{50} [μM] ^[b,c]
2a	-CH ₂ -4-hydroxyphenyl (S)	3.00
3a	-CH ₂ -4-hydroxyphenyl (S)	0.85
2b	-CH ₂ -3-indolyl (R)	12.0
3b	-CH ₂ -3-indolyl (R)	(67)
2c	-CH ₂ -2-naphthyl (R)	2.29
3c	-CH ₂ -2-naphthyl (R)	— ^[c]

[a] Chemically resynthesized compounds. [b] In parenthesis: %inh at $100 \mu\text{M}$. [c] IC_{50} value represents the mean value of two to four independent measurements. [c] Insoluble compound.

Binding of Potent KTGS-Identified ERAP2 Inhibitor **3a**

The X-ray cocrystal structure of **3a** with ERAP2 was solved (Figures 4, S6, Table S1).^[22] In the first crystal asymmetric unit (Figure 4a), hydroxamate moiety of **3a** chelates the zinc ion and interacts with adjacent side chains of residues Asp337, Asp 371. The hydroxyl of the phenol group makes a hydrogen bond with Arg895. The phenol ring lies between

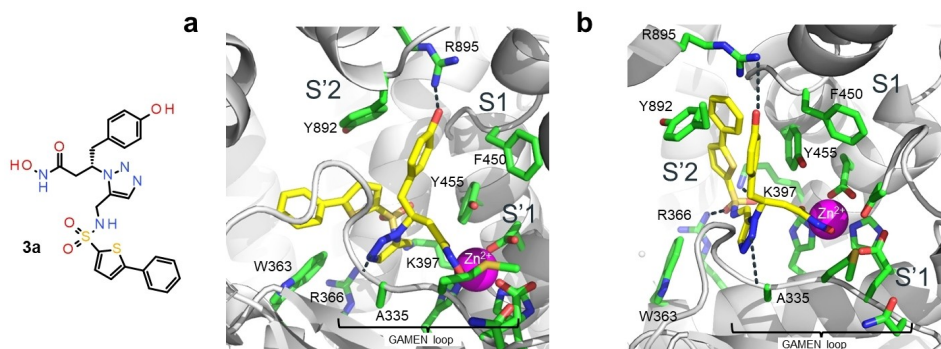


Figure 4. **3a** in the active site of ERAP2 (PDB: 7NUP),^[22] **3a** in chain A of ERAP2 (a) or in chain C (b) of the asymmetric unit, at 3.1 Å resolution. ERAP2 is shown in cartoon representation in light gray. c) Structure of **3a**. **3a** (C: yellow, S: dark yellow, O: red, N: blue) and selected residues (C: green, S: dark yellow, O: red, N: blue) in close proximity to **3a** are shown as sticks. Zinc ion is shown as a magenta sphere. The GAMEN loop, pockets S1, S'1 and S'2 are indicated. Hydrogen-bond interactions are represented as dashed lines. Images were generated using PyMOL™ Molecular Graphics System v1.3.

Tyr 892 and Phe450. The sulfonamide engages in hydrogen bonds with Lys397 via its oxygen atoms.

The triazole ring stacks with the thiophene and forms a hydrogen bond with the backbone NH of Ala335 of the aminopeptidase consensus sequence GAMEN, that is important in the formation of the transition state complex. The phenyl ring is involved in a T-shaped interaction with Trp363 (distance 3.7 Å). In the second crystal asymmetric unit (Figure 4b), **3a** adopts a U-shape as the 5-phenylthiophene group flips towards the S'2 pocket where it forms a T-shaped edge-to-face interaction with the phenol ring. The sulfonamide makes hydrogen bonds with both Lys397 and Arg366.

Structure-Activity Relationships Around KTGS Hits: Toward Single-Digit Nanomolar Inhibitors

Excited by these results, we further explored modifications around most potent inhibitor **3a** and its 1,4-triazole regioisomer **2a** (Table 2). In the 1,4-triazole series, shortening of the hydroxamic tail led to the submicromolar analog **4a** ($IC_{50}=0.76 \mu M$) whereas 1,5-triazole **5a** is less potent than its longer counterpart **3a** (Table 2). Replacement of the phenol group by an indole (**4b**) led to a complete loss of activity while replacement of the phenyl substituent of the thiophene by a pyridyl further increased activity (**4c**), underlining the importance of these two substituents in the binding. O-substitution of the phenol group by either a methyl or a phenyl (**4d-f**, Table 2). enhances drastically the potency in comparison with phenol counterparts, in particular in combination with the introduction of the pyridine ring on the thiophene (Table 2). Taken together, 2-pyridyl analogue **4e** is the best ERAP2 inhibitor

Table 2: Inhibition of ERAP2 by selected analogues **4a-f**, **5a**.

Cpd.	R1	R	IC_{50} [μM] ^[a,b]
4a	-CH ₂ -4-hydroxyphenyl (S)	-5-phenyl	0.76
5a	-CH ₂ -4-hydroxyphenyl (S)	-5-phenyl	3.28
4b	-CH ₂ -3-indolyl (R)	-5-phenyl	(43)
4c	-CH ₂ -4-hydroxyphenyl (S)	-5-(2-pyridyl)	0.47
4d	-CH ₂ -4-methoxyphenyl (S)	-5-phenyl	0.019
4e	-CH ₂ -4-methoxyphenyl (S)	-5-(2-pyridyl)	0.0039
4f	-CH ₂ -4-phenoxyphenyl (S)	-5-(2-pyridyl)	0.035

[a] In parenthesis: %inh at 100 μM . [b] IC_{50} value represents the mean value of two to four independent measurements.

so far described achieving single-digit nanomolar potency ($IC_{50}=3.9$ nM).

Understanding Key Interactions for Binding

To rationalize the 2-log potency increase between **4e** and analogues **4c** and **3a** we studied the binding of both **4c** and **4e** to ERAP2 via X-ray co-crystallography (PDB: 7NSK and 7HS0 respectively).^[23,24]

The shortening of the alkyl chain bearing the hydroxamic acid in **4c** in comparison to **3a**, induces a different binding in ERAP2 (Figure 5, S7) as the phenol ring points now towards the S'1 pocket. In chain A (Figure 5a), the phenol ring stacks with His370. The triazole ring makes a water-mediated hydrogen bond with Asp197 and stacks with the thiophenyl ring. The NH of the sulfonamide interacts with the aromatic ring of Phe450 while the oxygen atom of the sulfonamide makes a hydrogen bond with the backbone NH of Asn447. Pyridine lies in the vicinity of Tyr892 in the S'2 pocket. In chain B (Figure 5b), the phenol ring of **4c** stacks with His370 and is engaged in a network of hydrogen bonds with water Glu400 and Lys397 via its hydroxyl group. The NH of the sulfonamide interacts with aromatic ring of Phe450 while the oxygen atom of the sulfonamide makes a hydrogen bond with NH_2 of Asn447. The pyridine forms a hydrogen bond with Tyr455 and almost forms a π - π stacking interaction with Tyr892.

The hydroxamate moiety of **4e** chelates the zinc ion and interacts via its carbonyl group with the phenol of Tyr455 (Figure 6a,b, Table S3, Figure S8). The NH of the sulfonamide interacts with the aryl group of Phe450. The pyridyl ring stacks perfectly with Tyr892 and the triazole ring is engaged in hydrophobic contacts with Pro333 (3.90 Å). The phenoxyethyl group fits very nicely the hydrophobic pocket delimited by His370, Val367 and Trp363. Introduction of the methyl on the phenyl group optimized the binding of **4e** to ERAP2.

A comparison of pyridyl analogues **4e** (chain B) and **4c** (chains A, left panel, and B, right panel) bound to ERAP2 (Figure S9) shows that the two inhibitors adopt overall

similar U-shapes, with some key differences. First, while the phenoxyethyl group of **4e** is anchored in the S'1 pocket defined by Trp363, Val367, His370, Lys397, Glu400. This binding mechanism is not possible for **4c** owing to the absence of a terminal methyl group. The phenol group of **4c** (right panel), however, makes a stabilizing hydrogen bond to Glu400 and Lys97 via a water molecule in chain B. The displacement of this water molecule from its rather hydrophobic environment by **4e**, using methyl substitution of the phenol, can also contribute highly to its better binding to ERAP2.^[25,26] Second, while the pyridyl ring of **4e** is optimally stacked against Tyr892, the same ring adopts a different orientation in chain B of **4c** (right panel) (see also Figure 6), altering the network of hydrophobic contacts to Tyr892. Taken together, the terminal phenoxyethyl and pyridyl groups of **4e** are critical in positioning the two ends of the inhibitor optimally in the active site of ERAP2. This also restricts the conformational flexibility of **4e** which displays nearly identical conformations in both asymmetric units of the crystal structure (see also Figure S8), in contrast to **4c** (Figure 5) and allows optimal interaction of triazole and hydroxamic acid with Pro333 and zinc. These differences overall are significant in enhancing the potency of **4e** relative to **4c** (Table 2).

Improving Interaction with Non-Conserved Residues Drives Selectivity

We then explored the selectivity of a subset of ERAP2 inhibitors with various potencies (Figure 7). First, the study of selectivity towards closely related ERAP1 and IRAP enzymes (Figure 7a) shows that compounds are selective for ERAP2 over ERAP1 (selectivity between 30- and 1500-fold). Derivatives of beta-amino-acids like **2a** or **3a** are selective for IRAP. Shifting from the beta series ($n=1$) towards alpha series ($n=0$) greatly improves selectivity towards ERAP2, with **4d-f** displaying the best selectivity index (>150). We extended the selectivity study on additional enzymes like APN also from the M1 family, representative MMPs, TACE and LAP3 (Figure 7b). All

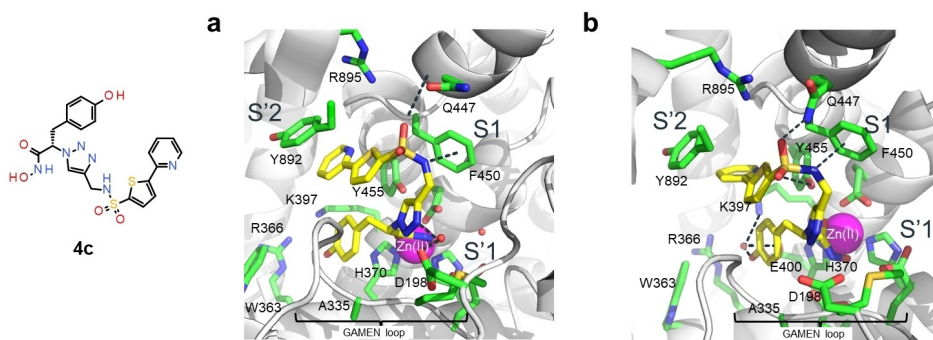


Figure 5. **4c** in the active site of ERAP2 (PDB: 7NSK).^[23] **8c** in chain A of ERAP2 (a) or in chain B (b) of the asymmetric unit, at 3.1 Å resolution. ERAP2 is shown in cartoon representation in light grey. **4c** (C: yellow, S: dark yellow, O: red, N: blue) and selected residues (C: green) in close proximity to **4c** are shown as sticks. Zinc ion is shown as a magenta sphere. The GAMEN loop, pockets S1, S'1 and S'2 are indicated. Hydrogen-bond interactions are represented as dashed lines. Images were generated using PyMOL™ Molecular Graphics System v1.3.

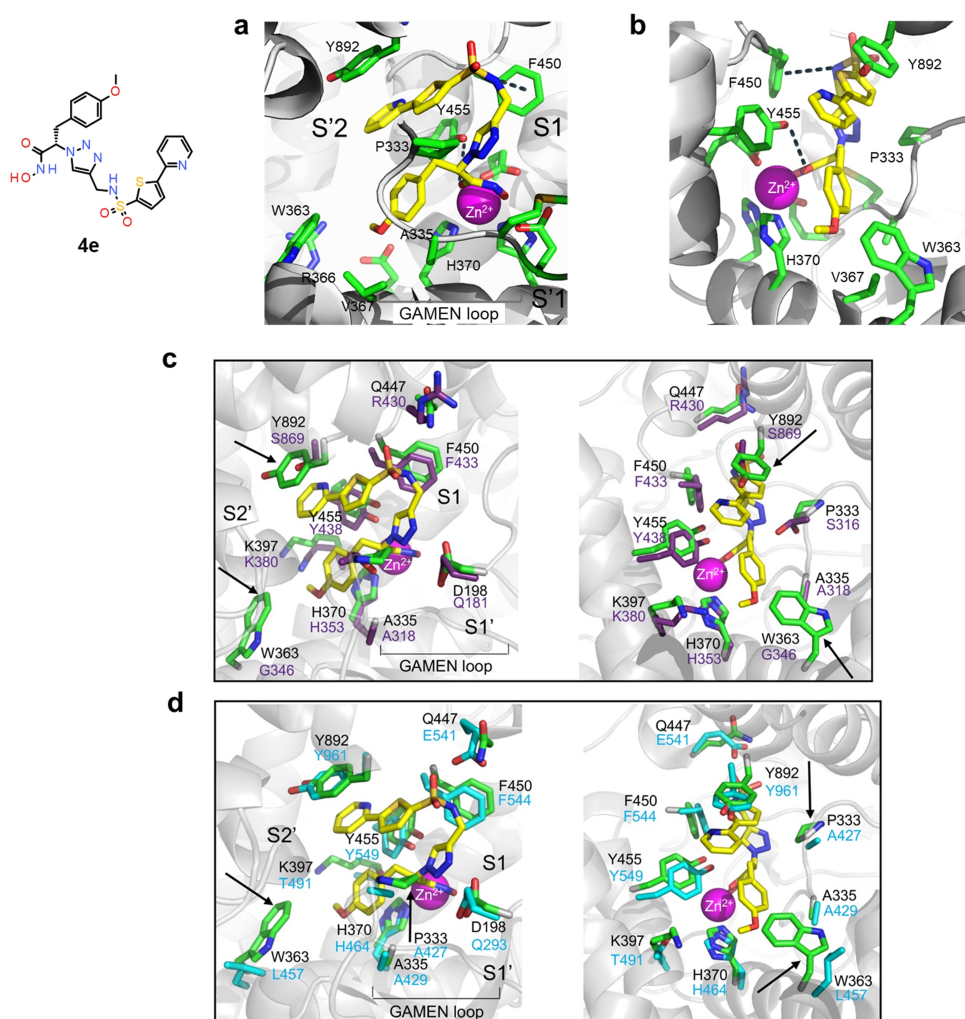


Figure 6. Compound **4e** in the active site of ERAP2 and superimposition with ERAP1 and IRAP. a,b) **8e** in chain B of the asymmetric unit of ERAP2 (PDB code 7HS0) at 3.2 Å;^[24] c,d) Superimposition of active-site residues of ERAP2-**4e** (PDB code 7HS0, in green) with homologous c) ERAP1 (PDB code 6Q4R, purple) and d) IRAP (PDB code 5MJ6, cyan) with views similar to a) and b). ERAP2 is shown in cartoon representation in grey and **8e** is shown in yellow sticks (C: yellow, S: dark yellow, O: red, N: blue). The zinc ion is shown as a magenta sphere. Selected residues of ERAP2/ ERAP1/IRAP in close proximity to **4e** are shown in sticks (C: green (ERAP2) or purple (ERAP1) or cyan (IRAP), O: red; N: blue). The GAMEN loop and approximate location of the specificity pockets S1, S1', and S2' are indicated. The black arrows indicate differences in key residue between the enzymes that could impact inhibitor binding. Hydrogen-bond interactions are represented as dashed lines. Images were generated using PyMOL™ Molecular Graphics System v1.3.

compounds are selective towards ERAP2. **4e**, which is the most potent ERAP2 inhibitor, is also the most selective (Figure 7c).

To rationalize the selectivity, we superimposed the ERAP2-compound co-crystal structures of **4e**, **3a** or **4c** with ERAP1 (PDB code 6Q4R) and IRAP (PDB code 5MJ6) (Figures 6c,d, S10, S11). Though the binding of all three compounds is different in ERAP2, they all interact with the ERAP2 selectivity residues Tyr892 or Arg895 in S2' via either the phenol ring (**3a**) or the phenyl/pyridyl ring (**4c**, **4e**). These residues are replaced in ERAP1 by Ser869 and Ser867, respectively (Figure 6c, S10, S11). The substitution of Tyr892 by a serine eliminates key hydrophobic interactions with the phenyl or pyridyl ring in all three inhibitors, reducing their selectivity for ERAP1. On the contrary, in IRAP, Tyr892 is conserved as Tyr961. For **3a**, the inter-

action of phenol with Arg895 in ERAP2 can be replaced by a hydrogen bond between Glu541 with phenol. Also, Phe550 unique to IRAP can make interactions with thiophene (Figure S10b, right), explaining the high activity of **3a** on IRAP.

When shortening the backbone by one methylene moiety (**4c**), the phenol ring points towards S2'–S1' and the sulphonamide points towards conserved Phe450 and the biaryl system points towards the side-chains of Tyr892–Tyr961. In **4e**, the terminal phenoxyethyl group forms hydrophobic interactions with Trp363 (Figures 6a,d). These important interactions are absent in IRAP because Trp363 is substituted to Leu457 where the Leu side chain points away from the phenoxyethyl group (Figure 6d). Furthermore, the substitution in IRAP of Pro333 to Ala427 abolishes hydrophobic interactions of the thiophenyl and

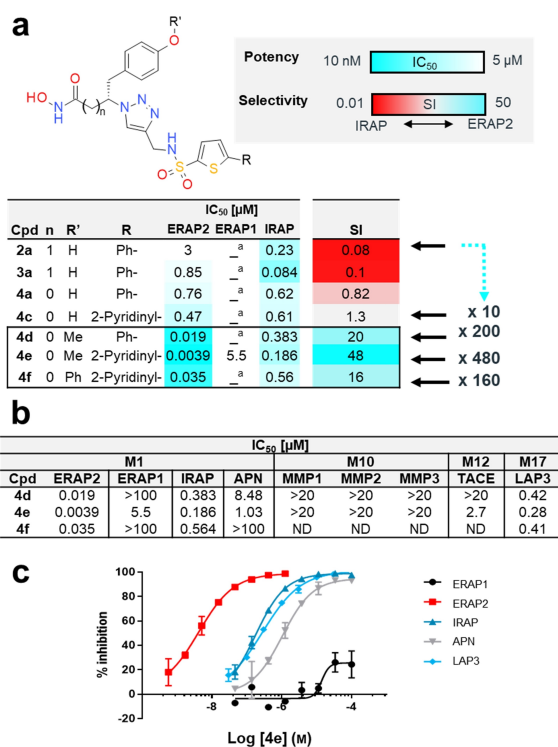


Figure 7. Selectivities towards related and distant metalloproteases. a) Selectivities towards ERAP1 and IRAP. IC₅₀ > 100 μM; SI = selectivity index; IC₅₀ on IRAP/IC₅₀ on ERAP2; b) Selectivities of **4d–f** on a panel of metalloproteases; ND = not determined; c) Dose-response curves for **4e**. IC₅₀ are mean of two to four independent measurements.

inhibitor backbone. As such, and relative to **4c**, **4e** binds more selectively to ERAP2 than to IRAP (Figure 7a).

Inhibitors Engage ERAP2 in Cells and Display Dose-Dependent Effect in a Whole-Cell Antigen Presentation Assay

Prior to cellular assays, we showed that **4d–4f** are inhibitors of ERAP2-mediated hydrolysis of two nonapeptides precursors of SIINFEKL, an ovalbumine-derived antigen, in a dose dependent manner. (Figure S12).

K_i calculated from competition assays with the Cheng–Prusoff equation were comparable to those using the shorter model substrate (Table S3). To examine direct target engagement for ERAP2, we performed Cellular Thermal Shift Assay (CETSA) in HEK cells under inhibitor-saturated conditions (Figure 8a,b). In cells, both **4d** and **4f** stabilize ERAP2 ($\Delta T_m = 3.52^\circ\text{C}$ and 1.81°C , respectively) more effectively than **4e**, consistently with the cell-permeability of compounds (Table S4). The Occupancy Concentration 50 (OC₅₀) measured in an isothermal dose-response fingerprints (ITDRF) for **4d** is 23 μM (Figure 8c).

4d and **4f** then showed a dose-dependent effect in a model of antigenic presentation in HEK cells where LSINFEKL is endogenously produced (Figure 8d). In this assay **4d** and **4f** display similar potency but better efficiency than those of the reference inhibitor leucinethiol. Noteworthy, at 50 μM, a concentration that engages 80 % of ERAP2 (Figure 8c) in cells, **4d** inhibits more than 60 % of the presentation of SIINFEKL.

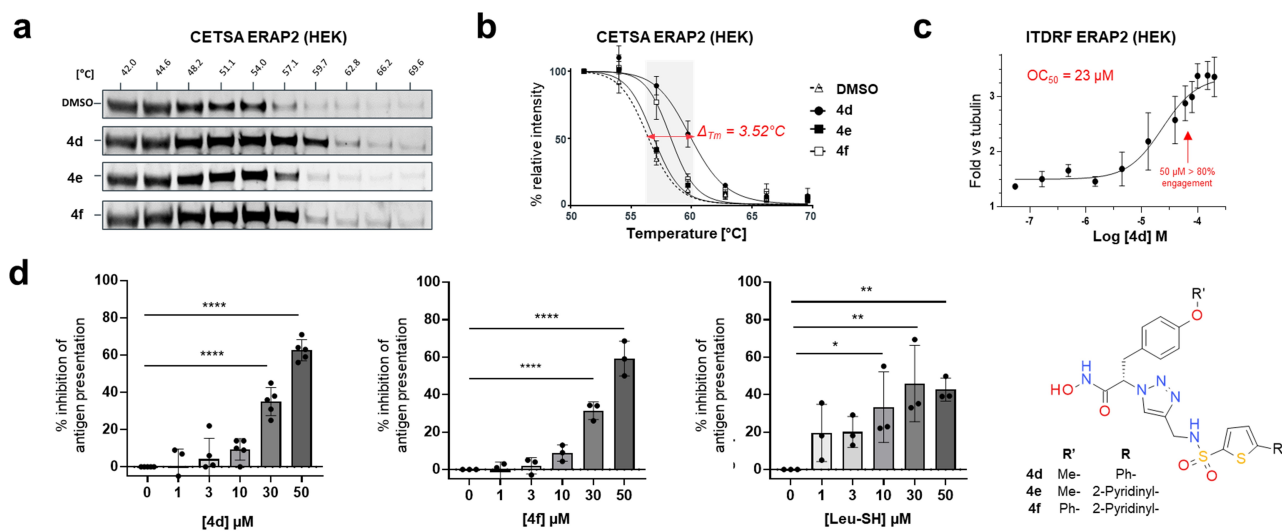


Figure 8. a–c) Target engagement of ERAP2 by **4d–f** in HEK cells using CETSA (Cellular Thermal Shift Assay), a) Representative western blots showing thermostable ERAP2 following indicated heat shocks in the presence of DMSO, **4d**, **4e** and **4f** at 30 mM. b) Quantification of thermostable ERAP2 obtained by three independent experiments ($n = 3$) \pm SD. Stabilization of ERAP2 in the presence of **4e** is expressed as the ΔT_m . c) Dose-dependent stabilization of ERAP2 by CETSA ITDRF (isothermal dose-response fingerprint) at 56°C ; OC₅₀ = 23 μM concentration at which 50% of ERAP2 is occupied by **4d** in cell. $n = 3$, normalized to tubulin. d) Dose-dependent effect of **4d** and **4f**, and Leucinethiol on SIINFEKL OVA-derived antigen presentation in HEK cells at 24 h, from at least three independent experiments ($n \geq 3$) \pm SD. Asterisks show statistical significance assessed by one-way ANOVA, Post-Hoc Dunnett for multiple comparisons with DMSO control, **** $p < 0.0001$, *** $p < 0.001$, ** $p < 0.01$, * $p < 0.05$.

ADME/PK Characterization of the Most Potent Inhibitors

Next, **4d–4f** were characterized regarding relevant in vitro ADME properties (Table 3). Pyridyl analogue **4e** is the least lipophilic analogue. All compounds are stable in plasma and in liver microsomes (half-lives > 6 h, > 40 min respectively).

Given its moderate $\log D_{(7.4)}$ and its target engagement properties, **4d** was selected to evaluate its in vivo pharmacokinetics in mice (Table 4). At a tolerated dose of 50 mg kg⁻¹, i.p., **4d** displays an AUC of 775 min μM and C_{max} in the range of OC₅₀.

Conclusion

The processing of antigen by ERAP enzymes is a key physiological process in immune response and it has been implicated in numerous diseases. Understanding and controlling this process to develop new therapeutic strategies requires potent and selective inhibitors. Until now, the study of ERAP2 has relied on genetic or transcriptional ablation,^[7,13] or non-selective inhibitors.^[17]

KTGS and more generally protein-templated reactions have been shown to provide potent hits and leads for drug discovery and chemical biology. Here we show that KTGS can also provide the basis for isoform selectivity. It allowed both the identification of the key thiophene sulfonamide and the key positioning of two groups in catalytic subsites without the requirement of an amino group. In summary, our strategy for identifying ERAP2 inhibitors demonstrates the significant value of KTGS to deliver potent and selective compounds from a set of reagents with designed restricted diversity. In particular we successfully optimized lipophilic ligand efficiency (LLE) of ERAP2 inhibitors discovered by KTGS **2a/3a** (LLE = 2.40–3.08 respectively) to identify the first nanomolar selective inhibitor **4e** (BDM88952, LLE = 5.92). Because analogue **4d** (BDM88951) displays outstanding subtype selectivity and adequate in vitro and in vivo properties, it can be used as a lead for future optimizations, exploration of the roles of ERAP2 and of the potential

Table 3: LogD, microsomal and plasma stability for selected compounds.^[a]

Cpd.	Log D _{7.4}	HLM Cl [μL min ⁻¹ g ⁻¹] (t _{1/2} [min])	H Plasma t _{1/2} [h]
4d	2.99	50 (> 40)	> 6
4e	1.81	21 (> 40)	> 6
4f	4.11	ND	> 6

[a] ND = not determined.

Table 4: Pharmacokinetic properties of **4d** in female mice i.p. 50 mg/kg.

T _{1/2} β [min]	C _{max} [μM]	T _{max} [min]	AUC _(0-∞) [min μM]
30	18	20	775

therapeutic utility of ERAP2 inhibitors, as cellular and animal models become available.

Acknowledgements

We thank Dr. Bernard Santarsiero for discussion and help with X-ray data collection of ERAP2-**4e** complex, and the staff at the Argonne National Laboratory, Argonne, IL, where these crystallographic data were collected. The authors acknowledge financial support from INSERM, University of Lille, Institut Pasteur de Lille, Region Hauts-de-France, l'Agence Nationale de la Recherche ANR grants ANR-20-CE18-0003-01, Institut Universitaire de France and FRM "Chemistry for Medicine Grant" DCM20181039548 (to R.D.P.), European Genomic Institute for Diabetes "E.G.I.D, ANR-10-LABX-0046, under the frame program Investissements d'Avenir I-SITE ULNE/ANR-16-IDEX-0004 ULNE (to B.D.), US National Institute of Allergy and Infectious Diseases grants R01 AI114467 and R01 AI108546 (to M.B.). The NMR facilities were funded by the Region Hauts-de-France, CNRS, Institut Pasteur de Lille, European Regional Fund (ERDF), Ministère de l'Enseignement supérieur, de la Recherche et de l'Innovation (MESRI) and Lille University. V.C. is a recipient of a PhD fellowship from the University of Lille and the University of Saarland. A.K.H.H. gratefully acknowledges funding from the European Research Council (ERC starting grant 757913) and the Helmholtz-Association's Initiative and Networking Fund.

Conflict of Interest

The authors declare no conflict of interest.

Data Availability Statement

PDB 7NSK, 7NUP and 7SH0 through <https://doi.org/10.2210/pdb7NUP/pdb>; <https://doi.org/10.2210/pdb7NSK/pdb>; <https://doi.org/10.2210/pdb7HS0/pdb> respectively. The data that support the findings of this study are available from the corresponding authors upon reasonable request.

Keywords: ERAP2 · Isoform Selectivity · Medicinal Chemistry · Metalloenzymes · Protein-Templated Reactions

- [1] I. Evnouchidou, P. van Endert, *Hum. Immunol.* **2019**, *80*, 290–295.
- [2] J. A. López de Castro, *Front. Immunol.* **2019**, *9*, 2463.
- [3] Y. Yao, N. Liu, Z. Zhou, L. Shi, *Hum. Immunol.* **2019**, *80*, 325–334.
- [4] M. Compagnone, L. Cifaldi, D. Fruci, *Hum. Immunol.* **2019**, *80*, 318–324.
- [5] J. A. L. de Castro, E. Stratikos, *Hum. Immunol.* **2019**, *80*, 310–317.
- [6] E. Lorente, M. G. Fontela, E. Barnea, A. J. Martín-Galiano, C. Mir, B. Galocha, A. Admon, P. Lauzurica, D. López, *Mol. Cell. Proteomics* **2020**, *19*, 994–1004.

- [7] W. J. Venema, S. Hiddingh, J. H. de Boer, F. H. J. Claas, A. Mulder, A. I. den Hollander, E. Stratikos, S. Sarkizova, L. T. van der Veken, G. M. C. Janssen, P. A. van Veelen, J. J. W. Kuiper, **2021**, *12*, 634441.
- [8] A. Wiśniewski, Ł. Matusiak, A. Szczerkowska-Dobosz, I. Nowak, W. Łuszczek, P. Kuśnierzcyk, *Hum. Immunol.* **2018**, *79*, 109–116.
- [9] I. Saule, S. V. Ibba, E. Torretta, C. Vittori, C. Fenizia, F. Piancone, D. Minisci, E. M. Lori, D. Trabattoni, C. Gelfi, M. Clerici, M. Biasin, *Front. Immunol.* **2020**, *10*, 1648–1648.
- [10] G. Stamatakis, M. Samiotaki, A. Mpakali, G. Panayotou, E. Stratikos, *J. Proteome Res.* **2020**, *19*, 4398–4406.
- [11] I. C. Kuo, H. K. Kao, Y. Huang, C. I. Wang, J. S. Yi, Y. Liang, C. T. Liao, T. C. Yen, C. C. Wu, K. P. Chang, *Oncotarget* **2017**, *8*, 61698–61708.
- [12] Y. W. Lim, H. Chen-Harris, O. Mayba, S. Lianoglou, A. Wuster, T. Bhangale, Z. Khan, S. Mariathasan, A. Daemen, J. Reeder, P. M. Haverty, W. F. Forrest, M. Brauer, I. Mellman, M. L. Albert, *Proc. Natl. Acad. Sci. USA* **2018**, *115*, E11701.
- [13] L. Saveanu, O. Carroll, V. Lindo, M. Del Val, D. Lopez, Y. Lepelletier, F. Greer, L. Schomburg, D. Fruci, G. Niedermann, P. M. van Endert, *Nat. Immunol.* **2005**, *6*, 689–697.
- [14] H. Chen, L. Li, M. Weimershaus, I. Evnouchidou, P. van Endert, M. Bouvier, *Sci. Rep.* **2016**, *6*, 28902.
- [15] A. Mpakali, P. Giastas, N. Mathioudakis, I. M. Mavridis, E. Saridakis, E. Stratikos, *J. Biol. Chem.* **2015**, *290*, 26021–26032.
- [16] A. Mpakali, P. Giastas, R. Deprez-Poulain, A. Papakyriakou, D. Koumantou, R. Gealageas, S. Tsoukalidou, D. Vourloumis, I. M. Mavridis, E. Stratikos, E. Saridakis, *ACS Med. Chem. Lett.* **2017**, *8*, 333–337.
- [17] E. Zervoudi, E. Saridakis, J. R. Birtley, S. S. Seregin, E. Reeves, P. Kokkala, Y. A. Aldhamen, A. Amalfitano, I. M. Mavridis, E. James, D. Georgiadis, E. Stratikos, *Proc. Natl. Acad. Sci. USA* **2013**, *110*, 19890–19895.
- [18] A. Papakyriakou, E. Zervoudi, S. Tsoukalidou, F. X. Mauvais, G. Sfyroera, D. C. Mastellos, P. van Endert, E. A. Theodorakis, D. Vourloumis, E. Stratikos, *J. Med. Chem.* **2015**, *58*, 1524–1543.
- [19] L. Medve, R. Gealageas, B. V. Lam, V. Guillaume, O. Castillo-Aguilera, V. Camberlein, C. Piveteau, M. Rosell, C. Fleau, S. Warengem, J. Charton, J. Dumont-Ryckembusch, D. Bosc, F. Leroux, P. van Endert, B. Deprez, R. Deprez-Poulain, *Eur. J. Med. Chem.* **2021**, *211*, 113053.
- [20] R. Deprez-Poulain, N. Hennuyer, D. Bosc, W. G. Liang, E. Enée, X. Marechal, J. Charton, J. Totobenazara, G. Berte, J. Jahklal, T. Verdelet, J. Dumont, S. Dassonneville, E. Woitrain, M. Gauriot, C. Paquet, I. Duplan, P. Hermant, F.-X. Cantrelle, E. Sevin, M. Culot, V. Landry, A. Herledan, C. Piveteau, G. Lippens, F. Leroux, W.-J. Tang, P. van Endert, B. Staels, B. Deprez, *Nat. Commun.* **2015**, *6*, 8250.
- [21] D. Bosc, V. Camberlein, R. Gealageas, O. Castillo-Aguilera, B. Deprez, R. Deprez-Poulain, *J. Med. Chem.* **2020**, *63*, 3817–3833.
- [22] A. Mpakali, P. Giastas, E. Stratikos, **2022**, Endoplasmic Reticulum Aminopeptidase 2 Complexed with a Hydroxamic Ligand, <https://doi.org/10.2210/pdb7NSK/pdb>.
- [23] A. Mpakali, P. Giastas, E. Stratikos, **2022**, Endoplasmic Reticulum Aminopeptidase 2 Complexed with a Mixed Hydroxamic and Sulfonyl Ligand, <https://doi.org/10.2210/pdb7NUP/pdb>.
- [24] M. Bouvier, L. Li, **2022**, Crystal Structure of Endoplasmic Reticulum Aminopeptidase 2 (Erap2) Complex with a Highly Selective and Potent Small Molecule, <https://doi.org/10.2210/pdb7HS0/pdb>.
- [25] S. T. Wroblewski, R. Moslin, S. Lin, Y. Zhang, S. Spengel, J. Kempson, J. S. Tokarski, J. Strnad, A. Zupa-Fernandez, L. Cheng, D. Shuster, K. Gillooly, X. Yang, E. Heimrich, K. W. McIntyre, C. Chaudhry, J. Khan, M. Ruzanov, J. Tredup, D. Mulligan, D. Xie, H. Sun, C. Huang, C. D'Arienzo, N. Aranibar, M. Chiney, A. Chimalakonda, W. J. Pitts, L. Lombardo, P. H. Carter, J. R. Burke, D. S. Weinstein, *J. Med. Chem.* **2019**, *62*, 8973–8995.
- [26] J. Schiebel, R. Gaspari, T. Wulsdorf, K. Ngo, C. Sohn, T. E. Schrader, A. Cavalli, A. Ostermann, A. Heine, G. Klebe, *Nat. Commun.* **2018**, *9*, 3559.

Manuscript received: March 8, 2022

Accepted manuscript online: July 29, 2022

Version of record online: August 19, 2022